Open access • Journal Article • DOI:10.1158/0008-5472.CAN-20-2756

Cancer-Associated Fibroblasts Promote Aggressive Gastric Cancer Phenotypes via Heat Shock Factor 1-Mediated Secretion of Extracellular Vesicles. — Source link

Nil Grunberg, Meirav Pevsner-Fischer, Tal Goshen-Lago, Judith Diment ...+16 more authors

Institutions: Weizmann Institute of Science, Rambam Health Care Campus, Kaplan Medical Center, University of Michigan ...+3 more institutions

Published on: 05 Feb 2021 - Cancer Research (American Association for Cancer Research (AACR))

Topics: Cancer, Tumor microenvironment, HSF1, Stromal cell and Cancer cell

Cancer-associated fibroblasts promote aggressive gastric cancer phenotypes via heat shock factor 1-mediated secretion of extracellular vesicles

Cancer-Associated Fibroblasts Promote Aggressive Gastric Cancer Phenotypes Via Heat Shock Factor 1-Mediated Secretion of Extracellular Vesicles

Nil Grunberg[1], Meirav Pevsner-Fischer[1], Tal Goshen-Lago[2], Judith Diment[3], Yaniv Stein[1], Hagar Lavon[1], Shimrit Mayer[1], Oshrat Levi-Galibov[1], Gil Friedman[1], Yifat Ofir-Birin[1], Li-Jyun Syu[4], Cristina Migliore[5], Eyal Shimoni[6], Salomon M. Stemmer[7,8], Baruch Brenner[7,8], Andrzej A. Dlugosz[4,9], David Lyden[10], Neta Regev-Rudzki[1], Irit Ben-Aharon[2,11], and Ruth Scherz-Shouval[1]

ABSTRACT

Gastric cancer is the third most lethal cancer worldwide, and evaluation of the genomic status of gastric cancer cells has not translated into effective prognostic or therapeutic strategies. We therefore hypothesize that outcomes may depend on the tumor microenvironment (TME), in particular, cancer-associated fibroblasts (CAF). However, very little is known about the role of CAFs in gastric cancer. To address this, we mapped the transcriptional landscape of human gastric cancer stroma by microdissection and RNA sequencing of CAFs from patients with gastric cancer. A stromal gene signature was associated with poor disease outcome, and the transcription factor heat shock factor 1 (HSF1) regulated the signature. HSF1 upregulated inhibin subunit beta A and thrombospondin 2, which were secreted in CAF-derived extracellular vesicles to the TME to promote cancer. Together, our work provides the first transcriptional map of human gastric cancer stroma and highlights HSF1 and its transcriptional targets as potential diagnostic and therapeutic targets in the genomically stable tumor microenvironment.

Significance: This study shows how HSF1 regulates a stromal transcriptional program associated with aggressive gastric cancer and identifies multiple proteins within this program as candidates for therapeutic intervention.

Introduction

Gastric cancer is the fifth most common cancer and the third most lethal cancer, worldwide (1). Recent advances in treatment were made possible due to better classification of gastric cancer subtypes, but the prognosis of advanced gastric cancer remains poor and many patients get diagnosed at an advanced stage of the disease due to limited understanding of the underlying biology (2). There is an urgent need to better understand the molecular basis of this disease, and to identify biomarkers that may predict outcome and guide therapy.

Gastric cancer is a heterogeneous disease. Traditionally, anatomical location (true gastric vs. gastro-esophageal) and histologic characteristics (diffuse vs. intestinal; tubular vs. papillary) have been used to classify gastric cancer subtypes (2). Recent advances in molecular understanding have enabled classification of gastric cancer into different subtypes based on chromosomal instability, microsatellite instability, genomic stability, presence of Epstein–Barr virus, and epithelial–mesenchymal transition (EMT), which were associated with different survival outcomes (3–6). Mutations in *CDH1* and *KRAS*, and overexpression of HER2, EGFR, FGFR2, VEGF, were shown to contribute to disease progression and correlate with poor outcome (7, 8). Despite serving as valuable guides in deciphering the complexity of gastric cancer, there has been little success in applying these molecular classifiers to treatment stratification and development of targeted therapies (3). Prognosis in the clinic is still mostly evaluated on the basis of TNM staging (tumor size, lymph node involvement, and metastasis), and the standard of care for localized gastric cancer is surgical intervention combined with chemotherapy (7).

Increasing evidence over the past decade highlighted the indispensable contribution of the tumor microenvironment (TME) to disease progression and treatment resistance (9). The TME is comprised of various cell types, including endothelial cells, fibroblasts, macrophages, and lymphocytes, as well as extracellular matrix components (ECM; ref. 10). The immune microenvironment of gastric cancer has gained increasing attention over the last years, due to its potential effect on immunotherapy in patients with high microsatellite instability (11). Yet little is known about the contribution of cancer-associated fibroblasts (CAF) to gastric cancer progression and metastasis. CAFs are the most abundant cell type in a variety of carcinomas (12). They support cancer cells by modifying the ECM, promoting angiogenesis, and maintaining a chronic inflammatory state (12–17). In gastric cancer,

[1]Department of Biomolecular Sciences, The Weizmann Institute of Science, Rehovot, Israel. [2]Division of Oncology, Rambam Health Care Campus, Haifa, Israel. [3]Department of Pathology, Kaplan Medical Center, Rehovot, Israel. [4]Department of Dermatology, Rogel Cancer Center, University of Michigan, Ann Arbor, Michigan. [5] University of Torino, Department of Oncology, Candiolo; Candiolo Cancer Institute, FPO-IRCCS, Candiolo, Italy. [6]Department of Chemical Research Support, The Weizmann Institute of Science, Rehovot, Israel. [7]Institute of Oncology, Davidoff Cancer Center, Rabin Medical Center, Beilinson Hospital, Petah Tikva, Israel. [8]Sackler Faculty of Medicine, Tel Aviv University, Ramat Aviv, Tel Aviv, Israel. [9]Department of Cell & Developmental Biology, Rogel Cancer Center, University of Michigan, Ann Arbor, Michigan. [10]Children's Cancer and Blood Foundation Laboratories, Departments of Pediatrics, and Cell and Developmental Biology, Drukier Institute for Children's Health, Meyer Cancer Center, Weill Cornell Medicine, New York, New York. [11]Rappaport Faculty of Medicine, Technion, Haifa, Israel.

Note: Supplementary data for this article are available at Cancer Research Online (http://cancerres.aacrjournals.org/).

Corresponding Author: Ruth Scherz-Shouval, Department of Biomolecular Sciences, Weizmann Institute of Science, Ullmann Building 237, Rehovot, 76100, Israel. E-mail: ruth.shouval@weizmann.ac.il

Cancer Res 2021;XX:XX–XX

doi: 10.1158/0008-5472.CAN-20-2756

accumulation of CAFs is correlated with increased tumor size, invasion, and metastasis (18). Recently, the abundance of natural killer cells, endothelial cells, and CAFs was shown to predict chemotherapy benefit in gastric cancer (19). However, the specific genes and molecular events contributing to these protumorigenic effects are not well understood. To address this, we set out to map the transcriptional landscape of gastric CAFs. Using laser-capture microdissection (LCM) and RNA-sequencing (RNA-seq) of CAFs from patients with gastric cancer, we define a gene-signature associated with poor disease outcome. We characterize this signature using mouse models and co-culture assays, and show that components of this signature are regulated by the master transcriptional regulator heat shock factor 1 (HSF1; ref. 20), and secreted from CAFs via extracellular vesicles (EV). These fibroblast-derived EVs contribute to tumor growth in an HSF1-dependent manner. Together, our work provides a comprehensive map of gastric cancer stromal transcription with potential implications on prognosis and treatment.

Materials and Methods

Ethics statement

Clinical samples and patient data were collected following approval by the Rabin medical center Institutional Review Board (IRB, protocol no. 0297-11-RMC) with full exemption for consent form for anonymized samples. Human samples used for MxIF staining were obtained from the Israel National Biobank for Research (MIDGAM; https://www.midgam.org.il/) under IRB no. 6141-19-SMC. These samples were collected from patients who provided written informed consent for collection, storage, distribution of samples, and data for use in future research studies. All animal studies were approved by the Institutional Animal Care and Use Committee (IACUC protocol nos. 15310619-2, 15140619-3, 06690820-3).

Mice

Athymic nude mice were purchased from Harlan Biotech. These mice, the triple-transgenic *Lgr5-EGFP-IRES-CreERT2; R26-LSL-rtTA-IRES-EGFP; tetO-GLI2A* mice (iLgr5;GLI2A mice; ref. 21), *Hsf1* null mice, and their WT littermates (BALB/c × 129SvEV, by Ivor J. Benjamin; ref. 22) were maintained under specific-pathogen-free conditions at the Weizmann Institute's animal facility.

Cell lines and primary cell cultures

N87 gastric cancer cells were kindly provided by Yosef Yarden (WIS; originally from ATCC). N87 cells were transduced with GFP using a third-generation lentiviral system. MC38 colon cancer cells were kindly provided by Lea Eisenbach (WIS; originally from NCI). MC38 cells were transduced with mcherry-luciferase using a second-generation lentiviral system. Primary MEFs were produced from WT and *Hsf1* null mice. HFF cells were purchased from ATCC. MEFs, MC38 cells, and N87 cells were cultured in RPMI (#01-100-1A, Biological Industries) supplemented with 10% FBS (Invitrogen) and P/S (Biological Industries). HFF cells were cultured in DMEM (#01-052-1A, Biological Industries) supplemented with 15% FBS, 1.5% L-glutamine, and P/S. Cell lines were tested routinely for *Mycoplasma* using EZ-PCR Mycoplasma Test Kit (#20-700-20, Biological Industries). MEFs were used in passage 1. Other cell lines were maintained below passage 25.

Laser capture microdissection of human gastric cancer samples

LCM cohort patients were selected on the basis of patient outcome data (Supplementary Table S1). Stromal and cancer regions were marked by a trained pathologist blinded to clinical and outcome data to include >90% CAFs for stroma and >90% cancer cells for cancer. Gastric muscle, immune islands, and blood vessels were excluded from microdissection. FFPE slides were deparaffinized and stained using Arcturus Paradise Plus Staining Kit (#KIT0312J; Thermo Fisher Scientific) according to the instructions of the manufacturer. Slides were left to dry for 5 minutes at RT followed by microdissection using the Arcturus (XT) laser microdissection instrument (#010013097, Thermo Fisher Scientific). Infrared capture was used to minimize RNA damage. CapSure Macro LCM caps (#LCM0211, Thermo Fisher Scientific) were used to capture microdissected tissue. To obtain sufficient material from these highly degraded RNA samples, we performed microdissection from 6 to 10, 5 μm sections per sample. Microdissected tissue from each sample was pooled together, and kept on dry ice until RNA isolation using the RNeasy FFPE Kit (#73504, Qiagen) with one modification—proteinase K digestion at 56°C was carried out for 1 hour.

Library preparation, RNA-seq, and analysis of LCM samples

Libraries were prepared using the SMARTer Stranded Total RNA-Seq v2-Pico Input Mammalian Kit (#634415, Takara Bio USA) according to the instructions of the manufacturer. Libraries were sequenced on Illumina NextSeq 500, at 50M reads for stroma and 25M reads for cancer samples, to provide sufficient reads to pass quality control filters of RNA-seq. Principal component analysis (PCA) was performed on full RNA-seq datasets for each sample (for stroma and cancer samples, separately). After calculating the first three main PCs (PCA1–3), we used the Robust Mahalanobis distance function to exclude potential outlier samples (see GitHub https://github.com/privefl/bigutilsr, and refs. 23–25). These robust Mahalanobis distances are approximately Chi-square distributed, which enables deriving P values of outliers (Supplementary Table S2). Because we used three dimensions, we chose a P value threshold of 0.00111 (P value <0.01 with Bonferroni correction for multiple comparisons), which concluded that patient 5 is an outlier in PCA2 and PCA3. This patient was removed from all downstream analysis. Read counts of the 8 patients were normalized and tested for difference using DESeq2 (26). Hierarchical clustering was carried out using Pearson correlation with complete linkage and on differentially expressed genes (DEG), which were filtered with the following parameters: baseMean > 5, $P_{adj} < 0.1$ and |logfoldchange| > 1. Pathway analysis was performed using Metascape, significant pathways were determined if $P < 0.05$ and FDR < 0.5. STRING analysis was performed including all DEGs.

CAF isolation and RNA-seq from iLgr5;GLI2A mice

Gastric cancer was induced in iLgr5;GLI2A mice as described in ref. 21. Gastric tumors were harvested post mortem, washed, minced, and dissociated using a gentleMACS dissociator and enzymatic digestion with DMEM containing 3 mg/mL collagenase A (#11088793001, Sigma Aldrich) and 0.1 mg/mL Deoxyribonuclease I (#LS002007, Worthington) for 20 minutes at 37°C. The single cell suspension was washed, filtered using 100 μm cell strainer, and immunostained. Normal gastric fibroblasts or CAFs were collected on the basis of negative selection for ghost dye, CD45, EpCAM, and CD31 and positive selection for PDPN. RNA-seq was done by MARS-Seq as described in ref. 27. DEGs were filtered with the following parameters: baseMean > 5, $P_{adj} < 0.01$, and |logfoldchange| > 3. Pathway analysis was performed using Metascape, significant pathways were determined if $P < 0.05$ and FDR < 0.5.

Validation of the patient and iLgr5;GLI2A mouse stromal signatures in independent patient cohorts

Patient data from the TCGA, Singapore (GSE15460), KUGH_KUCM (GSE26942), and ACRG cohorts (GSE62254) were downloaded, individual gene values were transformed to *z*-scores and the average of all known genes per sample was used to determine scores for the upregulated and downregulated signatures. For the *INHBA-THBS1-THBS2* gene-signature individual, gene values were transformed to *z*-scores and the average of genes per sample was determined. Gene symbols were matched through Affymetrix Human Genome U133 Plus 2.0 Array or Illumina HumanHT-12 V4.0 expression bead chip. For patient cohorts GSE15460 and GSE62254, we could match 109 DEGs from the CAF_up_sig and CAF_down_sig; and for GSE26942, we could match 87 DEGs from the CAF_up_sig and CAF_down_sig (out of the total 129 DEGs). For the iLgr5;GLI2A mCAF_up_sig and mCAF_down_sig, 314 DEGs were matched in the GSE15460 and GSE62254 cohorts and 271 DEGs in the GSE26942 cohort (out of the total 361 DEGs). Median signature was calculated using patients with complete survival and signature information. Kaplan–Meier (KM) analysis of overall survival with log rank *P* value was performed for each cancer type or patient cohort on patients stratified by median expression of each of these signatures.

HSF1 scoring and analysis

Nuclear HSF1 staining in stroma and cancer cells of 72 patients was analyzed by a trained pathologist who was blinded to both patient outcome and clinical data. A scale of 0 to 3 (0–3: low ≤ 1; 1.5 < intermediate ≤ 2; high >2) was set by the pathologist and scores were given on the basis of nuclear staining of HSF1 in stroma and cancer cells (Supplementary Table S1). Tissue samples were obtained from surgical specimens. Patients diagnosed as stage 1 to 3 did not present with metastases at diagnosis. Eight patients diagnosed as stage 4 gastric cancer with metastases were omitted from further analysis. Overall survival was defined as the time from first diagnosis to death based on the clinical data outlined in Supplementary Table S1. The scores in cancer cells and CAFs showed different distributions. Therefore, for survival analysis of HSF1 activation in cancer cells, patients with low and intermediate scores were combined and compared with patients with high scores, whereas for survival analysis of HSF1 activation in CAFs, patients with high and intermediate scores were combined and compared with patients with low scores (Supplementary Table S1). One patient could not be scored for cancer and for CAF HSF1 due to insufficient tumor tissue and was therefore excluded from all statistical analyses. Two patients could not be scored for CAF HSF1 and were excluded from CAF HSF1 analysis. Stage 2/3 was scored as stage 2 in the final clinical analysis.

Co-injection of recombinant activin A and THBS2 with MC38 cancer cells into nude mice

MC38 (2×10^5) were incubated with either PBS, 2.5 μg of Activin A (#CYT-146, ProSpec), or 2.5 μg of THBS2 (#1635-T2, R&D Systems) and co-injected in a total volume of 100 μL subcutaneously into Nude mice (Harlan laboratories). Forty-eight hours later, a second dose of 2.5 μg recombinant protein was injected. Tumors were measured by caliper for size and mice were sacrificed at day 15 due to high burden in the Activin A group.

Co-injection of EVs with MC38 cancer cells into nude mice

MC38 cells (2×10^5) were co-injected with either PBS or 1^*1^{10} WT or *Hsf1* null EVs subcutaneously into Nude mice (Harlan laboratories). Forty-eight hours later, a second dose (5×10^9) of EVs was injected. Tumors were measured by caliper for size and the mice were sacrificed at day 17 due to high tumor burden.

Data availability statement

RNA-seq data of iLgr5;GLI2A mice and patient samples were deposited in Gene Expression Omnibus (GEO) and can be accessed via GSE162301 and GSE165211, respectively. All other data supporting the findings of this study are available from the corresponding author on reasonable request.

Results

CAFs express a transcriptional program that promotes malignancy and correlates with poor disease outcome in gastric cancer

Gastric CAFs have been attributed protumorigenic effects, however the genes contributing to these effects are largely unknown. Therefore, we mapped the transcriptome of gastric CAFs in the intratumoral stroma by laser capture microdissection (LCM) followed by RNA-seq (Supplementary Fig. S1A). We isolated and sequenced CAF-rich stromal regions from formalin-fixed paraffin-embedded (FFPE) tumor sections of 9 patients with gastric cancer (Supplementary Figs. S1B and S1C; Supplementary Table S1), representing favorable (survival) and poor prognostic (lethality) outcomes (Supplementary Table S3). PCA showed that stromal samples from these patients clustered on basis of disease outcome (**Fig. 1A**; Supplementary Fig. S1D), whereas cancer samples from the same patients did not (**Fig. 1B**; Supplementary Fig. S1E). Differential expression analysis of stromal samples (see Materials and Methods, Supplementary Table S2; Supplementary Figs. S1F and S1G) revealed 129 DEGs between favorable and poor outcome groups (**Fig. 1C**; Supplementary Table S3). ECM organization (involving genes such as *AEBP1, COL10A1, COL11A1, SPOCK1, THBS2, EMILIN1*, and *TPM2*), response to growth factors (*INHBA, FGFR1, HSPB1*), and mesenchymal cell proliferation (*LMNA, UACA*) were the most differentially upregulated pathways in the stroma of patients with poor outcome (compared with patients with favorable outcome; **Fig. 1C**; Supplementary Table S4). The humoral immune response (involving genes such as *LCN2, PGC, REG1A, ITLN1, BPIFB1*, and *BIRC3*), digestive tract development (*GATA6, ITGA6, CLDN18*), and tissue homeostasis (*LYZ, MUC6*) were most significantly downregulated in these patients' stroma, compared with patients with favorable outcome (**Fig. 1C**; Supplementary Table S4). Analysis of cancer samples from the same patients highlighted only 13 DEGs, and no significant differentially regulated pathways (Supplementary Table S3; Supplementary Fig. S1H).

The observed changes in stromal gene expression could be driven by differences in stromal abundance between the patient groups. To test this, we performed image analysis to quantify stroma, cancer, and immune regions in hematoxylin & eosin (H&E) stained FFPE sections from the patients. We found no significant difference in the percentage of stroma, cancer, and immune cells between the favorable and poor outcome patients, suggesting that it is not the abundance, but the transcriptional program that is different between the two groups (Supplementary Figs. S1I–S1L). These findings suggest that as tumors progress, stromal pathways involved in maintaining normal stomach functions are replaced by pathways resulting from tumor–stroma interactions that support tumor growth.

We next set out to test the correlation between our stromal signature and clinical characteristics in independent datasets. Because no pure gastric CAF datasets with reported disease outcome are available, to the best of our knowledge, we turned to published datasets from bulk

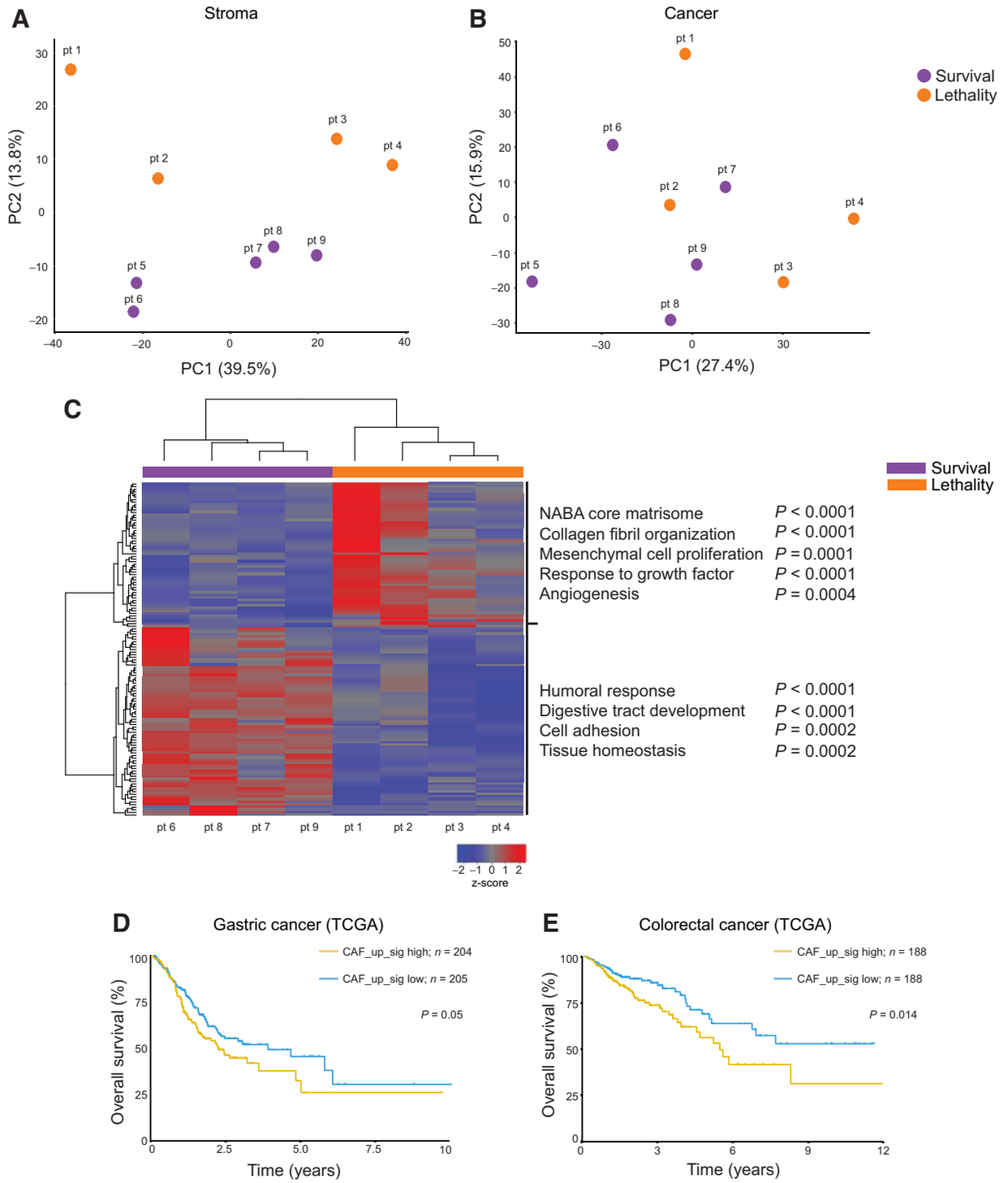

Figure 1.

The transcriptional landscape of gastric cancer stroma changes with disease aggressiveness. CAF-rich or cancer-rich regions of tumor sections from 9 patients with gastric cancer were laser-capture microdissected and analyzed by RNA-seq. PCA was performed for (**A**) CAFs and (**B**) cancer cells. Purple/orange dots—survival/lethality, as indicated. **C,** Heatmap showing hierarchical clustering of 129 genes differentially expressed in CAF-rich samples with favorable versus poor outcome. Pathway analysis was performed using Metascape. Selected significant pathways ($P < 0.05$, FDR < 0.5) are shown (see Supplementary Table S4). Purple/orange bars—survival/lethality, as indicated. **D** and **E,** Kaplan–Meier (KM) analysis showing overall survival of patients with (**D**) gastric or (**E**) colorectal cancer from the TCGA stratified on the basis of median expression of the stromal gene signature (CAF_up_sig).

tumors and asked whether a stromal signature comprised of genes upregulated in poor outcome patients in our dataset (CAF_up_sig) could be detected in bulk tumors (including both stroma and cancer cells). First, we analyzed The Cancer Genome Atlas (TCGA) datasets for gastrointestinal (GI) tract cancers (gastric, colorectal, pancreatic, hepatocellular, esophageal; **Fig. 1D–E**; Supplementary Table S5), and found that the CAF_up_sig is significantly associated with poor outcome in gastric cancer and in colorectal cancer (**Fig. 1D** and **E**). Genes downregulated in the stroma (CAF_down_sig) did not show any significant association with survival (Supplementary Figs. S1M and S1N).

We then analyzed datasets from three other large patient cohorts: The Singapore cohort, the KUGH_KUCM cohort, and the ACRG cohort (Supplementary Table S6). CAF_up_sig expression significantly associated with poor overall survival in the Singapore cohort and in the KUGH_KUCM cohort, and a similar trend was found with the ACRG cohort (**Fig. 2A–C**). Our CAF_down_sig showed an opposite trend – high expression of CAF_down_sig significantly correlated with favorable outcome in the Singapore and KUGH_KUCM cohorts, and a similar mild trend was observed with the ACRG cohort (**Fig. 2D–F**). Univariate analysis showed that CAF_up_sig expression, cancer stage, and presence of metastasis were associated with poor overall survival in the Singapore and the KUGH_KUCM cohorts and the ACRG cohort showed a similar trend (Supplementary Table S6).

We next looked for potential associations between expression of our CAF signature and gastric cancer subtypes. In all 3 patient datasets, CAF_up_sig expression, but not CAF_down_sig expression, was significantly enriched in the diffuse gastric cancer subtype, which typically has a worse prognosis compared with the intestinal subtype (**Fig. 2G–I**; Supplementary Figs. S2A–S2C). In addition to the histologic classification of gastric cancer to diffuse and intestinal subtypes, two independent molecular classification methods were described recently (4, 5): A mesenchymal phenotype (MP) characterized by high genomic integrity and associated with poor survival, and an epithelial phenotype (EP) characterized by low genomic integrity and associated with favorable survival, were identified in the KUGH_KUCM cohort (5); and four molecular subtypes (MSS $TP53^{-}$, MSS $TP53^{+}$, MSI, EMT) were characterized in the ACRG cohort, of which the EMT subtype was associated with the worst outcome (4). Analyzing the KUGH_KUCM cohort, we found that the CAF_up_sig was significantly enriched in the MP class, and the CAF-down_sig was significantly enriched in the EP class (**Fig. 2J**). In the ACRG cohort, the CAF_up_sig was significantly enriched in the EMT subtype while the CAF_down_sig was significantly enriched in MSS $TP53^{+/-}$ subtypes, associated with more favorable outcomes (**Fig. 2K**).

Supporting this classification, gene set enrichment analysis (GSEA) using MSigDB (Hallmark gene sets, see Supplementary Materials and Methods) on the full stromal RNA-seq dataset highlighted EMT as the most significantly enriched pathway in patients with poor outcome compared with patients with favorable outcome (Supplementary Figs. S2D; Supplementary Table S7). These analyses collectively indicate that the stromal signature correlates with diffuse, mesenchymal, and aggressive gastric cancer subtypes, further reinforcing the clinical relevance of our stromal classification and pointing to specific genes for dissection and targeting.

A transcriptional signature derived from mouse $PDPN^{+}$ gastric CAFs is associated with aggressive gastric cancer phenotypes and poor disease outcome in patients

To further dissect the contribution of CAFs to gastric cancer, we induced gastric cancer in mice using a triple-transgenic gastric cancer mouse model- Lgr5-EGFP-IRES-CreERT2; R26-LSL-rtTA-IRES-EGFP; tetO-GLI2A mice, (iLgr5;GLI2A mice; ref. 21). This model is based on deregulated activation of the Hedgehog pathway by expression of GLI2A, an activated form of GLI2, in *Lgr5* expressing stem cells in the stomach (21). We isolated CAFs and normal fibroblasts from the stomachs of gastric cancer-induced and naïve iLgr5;GLI2A mice, and performed RNA-seq to obtain a pure mouse CAF transcriptional signature (Supplementary Table S8). To that end tumors were excised 3 weeks after GLI2A induction, and CAFs were isolated by fluorescence activated cell sorting (FACS) based on negative selection for CD45 (immune), EpCAM (epithelial), and CD31 (endothelial cells), and positive selection for PDPN (fibroblasts; Supplementary Fig. S3A; Supplementary Table S9; refs. 16, 28, 29). A total of 154 genes were differentially upregulated and 207 were differentially downregulated in CAFs compared with normal gastric fibroblasts (Supplementary Table S8). Pathway analysis highlighted similar pathways to those discovered in the stromal dissection of the human patient samples: ECM organization (*Adam12, Acan, Lox*), activation of matrix metalloproteinases (*Mmp3, Mmp9, Mmp10, Mmp13*), response to growth factors (*Inhba, Grem1, Runx3*), and regulation of hormone levels (*Inhba, Cnr1, Cpe*) were among the most differentially upregulated pathways in mouse CAFs, whereas digestion (*Apoa1, Tff1, Pgc*) and tissue homeostasis (*Atp4a, Car2, Cldn18*) were the most differentially downregulated pathways compared with normal gastric fibroblasts (Supplementary Table S10). We then checked whether a signature comprised of genes upregulated in mouse CAFs (mCAF_up_sig) or genes downregulated in mouse CAFs (mCAF_down_sig) would be associated with clinical characteristics in the Singapore, KUGH_KUCM, and ACRG cohorts (Supplementary Table S11). Similar to the CAF_up_sig from patient samples, high expression of the mCAF_up_sig significantly associated with poor overall survival in the Singapore cohort and in the KUGH_KUCM cohort, and the ACRG cohort showed a similar trend that was not statistically significant (**Fig. 3A**; Supplementary Figs. S3B and S3C). The mCAF_down_sig showed an opposite trend—it was significantly associated with favorable outcome in the Singapore cohort and a similar trend was seen in the KUGH_KUCM cohort (**Fig. 3A**; Supplementary Fig. S3D). The ACRG cohort showed no particular trend for this analysis (Supplementary Fig. S3E). The mCAF_up_sig also correlated with the more aggressive MP and EMT molecular subtypes similar to the CAF_up signature from patient samples (**Fig. 3B**; Supplementary Fig. S3F), whereas the mCAF_down_sig correlated with the less aggressive EP and MSS $TP53^{+/-}$ subtypes (**Fig. 3B**; Supplementary Fig. S3G). Collectively, the findings obtained from pure mouse CAFs support our findings from patient samples, indicate that CAFs support gastric cancer and provide potential targets and experimental systems for further characterization in mouse and human.

INHBA and THBS1/2 are upregulated in gastric cancer stroma

To characterize stromal pathways highlighted by our transcriptional profiling, we queried our patient gene list for potential interactions of translated proteins using STRING (**Fig. 3C**). On the basis of this analysis we chose to focus on two targets upregulated in poor outcome patients: inhibin Subunit Beta A (INHBA) and thrombospondin 2 (THBS2), suggested to be part of a common signaling network (30). Both targets were recently found by us to be highly expressed in a subset of wound-healing CAFs in breast cancer (16). Moreover, they were both part of the EMT gene set highlighted by the GSEA analysis as enriched in patients with poor outcome (Supplementary Fig. S2D; Supplementary Table S7). We added to this analysis thrombospondin 1 (THBS1), a close homologue of THBS2 that showed a similar trend of

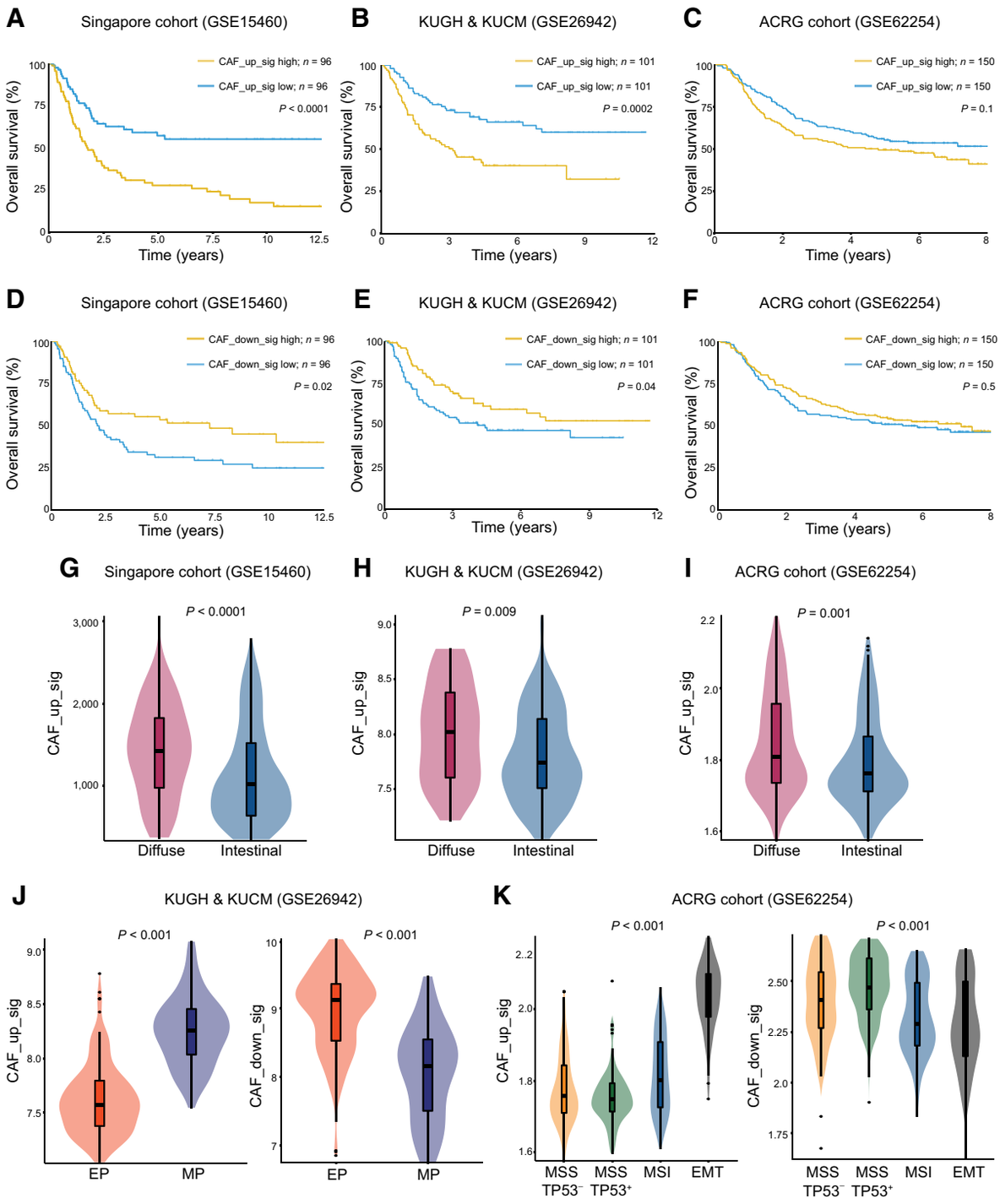

Figure 2.

High expression of the CAF signature is associated with aggressive disease and poor disease outcome in patients with gastric cancer. **A–C,** KM analysis showing overall survival of patients from (**A**) the Singapore cohort; (**B**) the KUGH & KUCM cohort; and (**C**) the ACRG cohort stratified on the basis of expression of the upregulated (CAF_up_sig) stromal gene signature. **D–F,** KM analysis showing overall survival of patients from the (**D**) Singapore cohort, (**E**) KUGH & KUCM cohort, and (**F**) ACRG cohort stratified on the basis of expression of the downregulated (CAF_down_sig) stromal gene signature. **G–I,** Enrichment of the CAF_up_sig (mean of normalized counts) in patients with diffuse versus intestinal gastric cancer in the (**G**) Singapore cohort; (**H**) KUGH & KUCM cohort; and (**I**) ACRG cohort. **J,** Enrichment of the CAF_up_sig and CAF_down_sig (mean of the normalized counts) in patients with MP and EP subtypes in the KUGH & KUCM cohort (5). **K,** Enrichment of the CAF_up_sig and CAF_down_sig (mean of normalized counts) in patients with molecular subtypes previously identified in the ACRG cohort (4). One-way ANOVA was used in **G–K**.

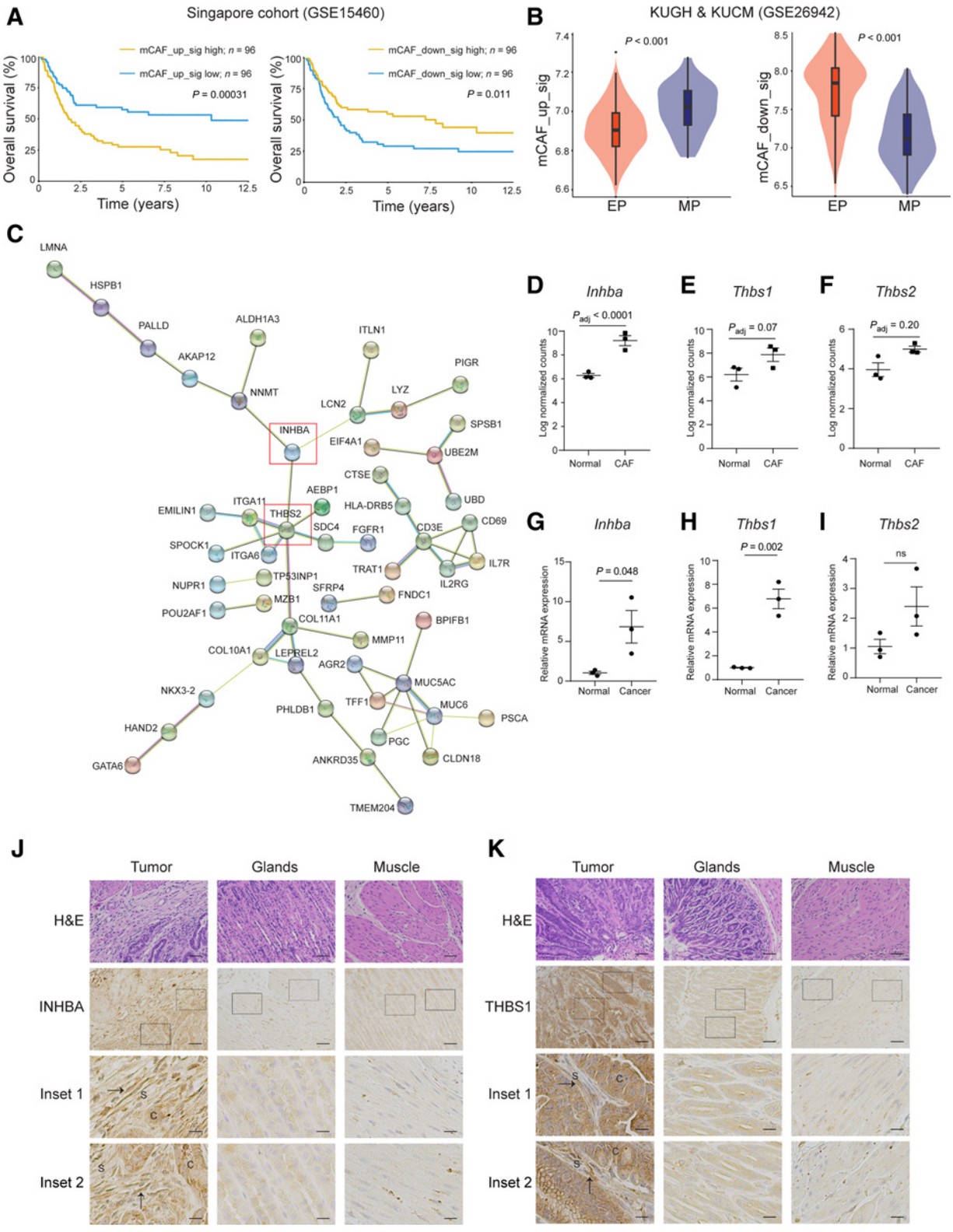
A
Singapore cohort (GSE15460)
mCAF_up_sig high; n = 96
mCAF_up_sig low; n = 96
P = 0.00031
Overall survival (%)
Time (years)
mCAF_down_sig high; n = 96
mCAF_down_sig low; n = 96
P = 0.011
B
KUGH & KUCM (GSE26942)
P < 0.001
mCAF_up_sig
mCAF_down_sig
EP
MP
C
LMNA
HSPB1
PALLD
ALDH1A3
AKAP12
NNMT
ITLN1
PIGR
LCN2
LYZ
SPSB1
INHBA
EIF4A1
UBE2M
CTSE
AEBP1
UBD
EMILIN1
ITGA11
THBS2
HLA-DRB5
CD69
SDC4
FGFR1
CD3E
SPOCK1
ITGA6
IL7R
TRAT1
TP53INP1
IL2RG
NUPR1
SFRP4
FNDC1
MZB1
POU2AF1
COL11A1
BPIFB1
MMP11
COL10A1
LEPREL2
AGR2
MUC5AC
NKX3-2
TFF1
MUC6
PSCA
PHLDB1
HAND2
PGC
CLDN18
GATA6
ANKRD35
TMEM204
D
Inhba
P_adj < 0.0001
Log normalized counts
Normal
CAF
E
Thbs1
P_adj = 0.07
F
Thbs2
P_adj = 0.20
G
Inhba
P = 0.048
Relative mRNA expression
Normal
Cancer
H
Thbs1
P = 0.002
I
Thbs2
ns
J
Tumor
Glands
Muscle
H&E
INHBA
Inset 1
Inset 2
S
C
K
Tumor
Glands
Muscle
H&E
THBS1
Inset 1
Inset 2
S
C

expression (Supplementary Table S3) and was also included in the enriched EMT gene set (Supplementary Table S7). *Inhba* was differentially upregulated also in mouse CAFs from iLgr5;GLI2A tumors, and Thbs1/2 showed a similar trend (**Fig. 3D–F**). INHBA is a subunit of Activin and Inhibin, dimeric proteins belonging to the TGFß superfamily (31, 32). Activin A is a homodimer of two INHBA subunits, whereas Inhibin A and Activin AB are heterodimers of INHBA with INHA and INHBB, respectively (32). INHBA is known to play a role in inflammation, tissue repair, and activation of myofibroblasts, and increased levels of INHBA are associated with lymph node (LN) metastasis, gastric cancer cell proliferation and chemoresistance (33). THBS1/2 are adhesive glycoproteins involved in cell–cell and cell–matrix interactions. Increased levels of THBS2 are associated with LN metastasis and increased invasion in gastric cancer (34). The role of THBS1 is less clear since it was implicated both in pro- and antitumorigenic activities in gastric cancer (35–37). Both INHBA and THBS1/2 are known to play an important role in gastric cancer, however their role in the TME is not well studied (30). To validate our RNA-seq results, we extracted total RNA from iLgr5;GLI2A tumors and examined the levels of *Inhba, Thbs1*, and *Thbs2* by qPCR. *Inhba* and *Thbs1* levels were significantly upregulated in gastric tumors compared with normal gastric tissue and *Thbs2* showed a similar trend (**Fig. 3G–I**). To define the tissue localization of INHBA and THBS1/2, and confirm their expression at the protein level, we performed IHC staining of sections from iLgr5;GLI2A tumors and from normal stomach controls using antibodies against INHBA and THBS1. INHBA and THBS1 were expressed at very low levels in normal gastric glands and muscle (**Fig. 3J** and K). Gastric tumors, however, exhibited high levels of INHBA and THBS1 both in stroma and in cancer cells (**Fig. 3J** and **K**). Together, these findings support our patient RNA-seq results and suggest that INHBA and THBS1/2 are upregulated in gastric cancer stroma.

Given their connectivity to other genes in the stromal network revealed by the STRING analysis (**Fig. 3C**), and the potential simplicity of a 3-gene signature (compared with a signature comprised of dozens of genes), we tested whether a minimal gene signature comprised of only *INHBA* and *THBS1/2* would correlate with disease outcome in our patient datasets. We found that the 3-gene signature (*INHBA/THBS1/THBS2*) correlated with poor disease outcome in the TCGA gastric cancer and colorectal cancer datasets, the Singapore cohort, and the KUGH_KUCM cohort (Supplementary Figs. S4A–S4D; Supplementary Table S6). As with the other stromal signatures that we analyzed, the ACRG cohort showed a similar trend of disease outcome that was not statistically significant (Supplementary Fig. S4E), possibly due to differences in patient follow up time or cohort characteristics (Supplementary Table S6). These results imply that stromal INHBA and THBS1/2 are associated with aggressive disease phenotypes in gastric cancer, and serve as attractive targets for characterization.

HSF1 activation in gastric CAFs is associated with poor disease outcome

In search for potential transcriptional regulators of the stromal signature in general, and INHBA and THBS1/2 in particular, we examined heat-shock factor 1 (HSF1). Previously, we and others have shown that HSF1, the master transcriptional regulator of the heat shock response, plays an important role in the conversion of fibroblasts into CAFs in the TME (20, 38). Moreover, *INHBA* and *THBS1* were shown to be transcriptional targets of HSF1 (39, 40). In gastric cancer, activation of HSF1 in cancer cells was shown to correlate with poor disease outcome (41), yet the contribution of stromal HSF1 to disease outcome has not been assessed. HSF1 translocates from the cytoplasm to the nucleus and binds to heat shock elements in the DNA upon activation (39). Therefore, its nuclear localization is commonly used as a proxy for HSF1 activation (39). Indeed, IHC staining of FFPE sections from patients with gastric cancer revealed nuclear HSF1 staining both in cancer cells and in CAFs, whereas normal stomach glands and muscle exhibited low or no HSF1 staining (**Fig. 4A**).

To systematically test whether stromal activation of HSF1 is associated with disease outcome in gastric cancer, we performed IHC staining for HSF1 and scored its nuclear localization in cancer cells and CAFs, in sections from 64 patients with gastric cancer (including the subcohort of LCM–RNA-seq patients) with documented clinical characteristics and patient outcome data (Supplementary Table S1). High HSF1 activation in cancer cells correlated with shorter overall survival time and stromal HSF1 showed a similar trend (**Fig. 4B** and **C**; Supplementary Table S12). In the cohort of patients analyzed by LCM and RNA-seq, all patients with poor outcomes also exhibited intermediate or high HSF1 activation (i.e., nuclear localization) in cancer and stromal cells, whereas patients with favorable outcomes differed in their HSF1 activation status (Supplementary Table S1). Interestingly, stromal HSF1 activation also significantly correlated with HER2 status —$HER2^-$ patients exhibited high HSF1 levels whereas $HER2^+$ patients had low stromal HSF1 activation levels (Supplementary Table S1). These results imply that in addition to its previously described roles in gastric cancer cells, HSF1 activates complementary pathways in gastric stroma that promote aggressive disease phenotypes. This conclusion was further supported by a multivariate Cox proportional hazards regression analysis (Supplementary Table S12). In an additive multivariate model considering tumor stage and HSF1 score, stromal HSF1 score and tumor stage were significantly associated with overall survival ($P = 0.006$), and this association was more significant than that of cancer HSF1 and tumor stage with survival ($P = 0.016$).

Stromal INHBA and THBS1/2 are targets of HSF1, *in vitro*

Multiplexed immunofluorescent staining (MxIF) of patient with gastric cancer samples showed that HSF1 is co-expressed with INHBA and THBS1, in cancer cells and in CAFs, whereas normal stomach

Figure 3.

INHBA and THBS1/2 are upregulated in gastric cancer. **A** and **B,** Gastric cancer was induced in iLgr5;GLI2A mice, $PDPN^+$ fibroblasts were isolated from the resulting tumors and RNA-seq was performed using fibroblasts isolated from stomachs of naïve mice as control. Signatures comprised of genes upregulated (mCAF_up_sig;) or downregulated (mCAF_down_sig) in $PDPN^+$ CAFs vs. $PDPN^+$ normal fibroblasts were derived. **A,** KM analysis of overall survival in patients from the Singapore cohort stratified on the basis of expression of the mCAF_up_sig (left) or mCAF_down_sig (right). **B,** Enrichment of the mCAF_up_sig and mCAF_down_sig (mean of normalized counts) in patients with the MP and EP subtypes in the KUGH & KUCM cohort. One-way ANOVA was used for statistical analysis. **C,** STRING analysis of potential interactions between protein products of genes differentially expressed in patients with gastric cancer with favorable versus poor outcome. Proteins with no connections were omitted from the image. THBS2 and INHBA are highlighted in red. **D–F,** Log-normalized counts and *P*-adjusted values of the indicated genes taken from DESeq analysis of the iLgr5;GLI2A $PDPN^+$ CAF RNA-seq data (Supplementary Table S8). **G–I,** Total RNA levels of the indicated genes normalized to HPRT in normal stomachs and tumors (cancer) from iLgr5;GLI2A mice. $N = 3$ mice per group, means ± SEM are presented. Two-tailed Student *t* test was used for statistical analysis. **J–K,** Representative images showing H&E and immunohistochemical staining of the indicated proteins in gastric tumors and control stomachs (naïve) from iLgr5;GLI2A mice. $N = 5$ mice for cancer and $N = 3$ mice for normal control. C, cancer; S, stroma. Scale bar = 100 µm. Arrows indicate INHBA and THBS1 positive CAFs.

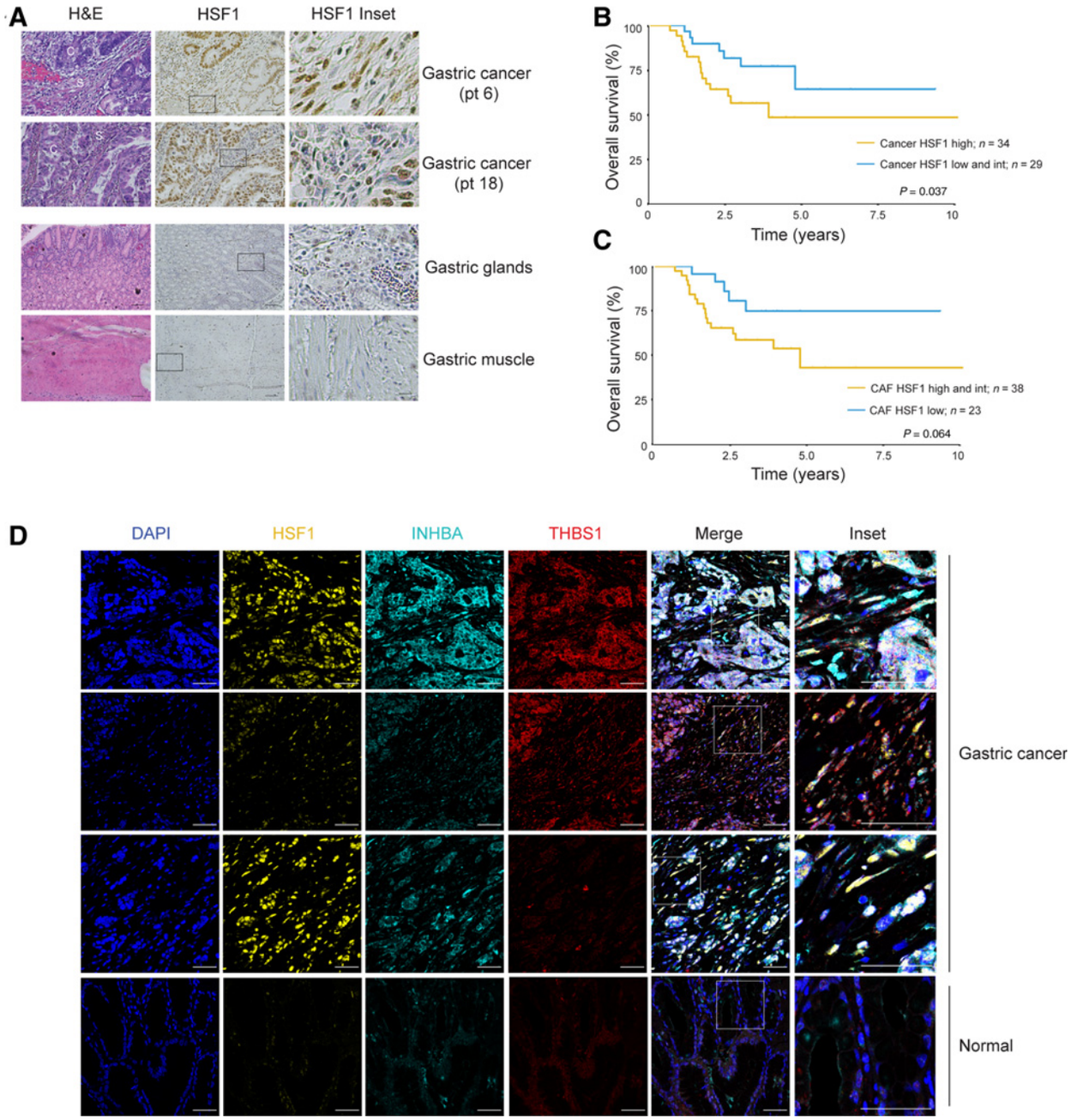

Figure 4.

HSF1 is co-expressed with INHBA and THBS1 in human gastric CAFs. **A,** FFPE sections from 64 patients with gastric cancer and four normal controls were stained by H&E and IHC staining for HSF1. (Top) Images representing high (pt 6) versus low (pt 18) nuclear HSF1 staining in CAFs. (Bottom) Representative images of normal gastric glands and muscle. C, cancer; S, stroma. Scale bar = 100 μm. **B** and **C,** 64 gastric cancer samples stained as described above were scored for high/intermediate (int)/low nuclear HSF1 staining in cancer cells/CAFs, and KM analysis of overall survival in these patients was performed. **B,** Patients were stratified by high versus int/low HSF1 scores in cancer cells. **C,** Patients were stratified by high/int versus low HSF1 scores in CAFs (see Supplementary Table S1). **D,** FFPE sections from 4 patients with gastric cancer and 2 normal stomach controls were stained by multiplexed immunofluorescence for HSF1, INHBA, THBS1, and DAPI (nuclear marker). Representative images from 3 different patients and one control are shown. Scale bar = 50 μm.

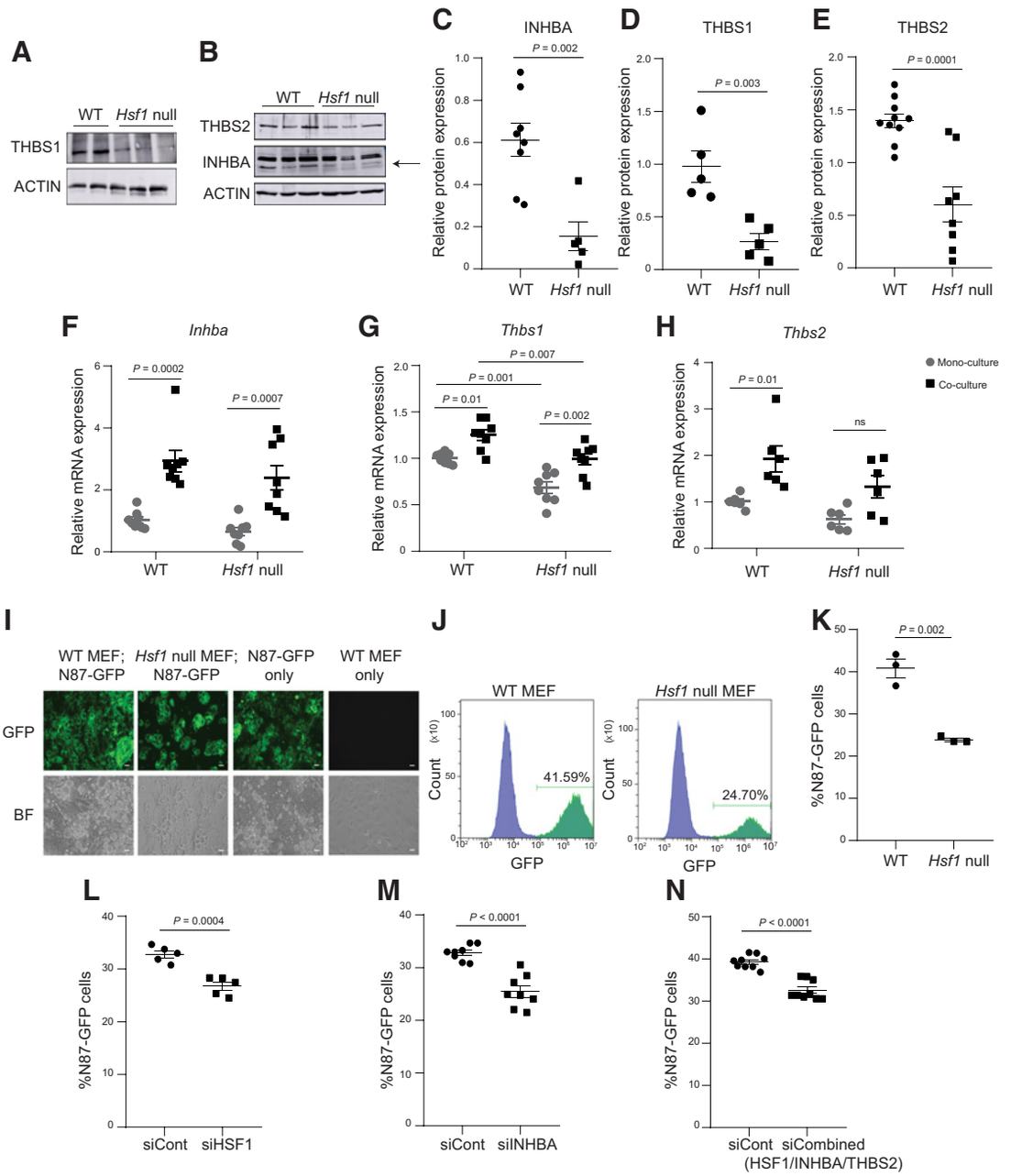

Figure 5.

Stromal INHBA and THBS1/2 expression is HSF1-dependent. **A–E,** INHBA, THBS1, and THBS2 protein expression levels in WT and *Hsf1* null primary MEFs were analyzed by Western blot analysis. Representative blots are shown in **A** and **B**. An arrow indicates the expected size of INHBA bands. **C,** INHBA Western blot analysis results of 5 to 10 biological replicates (across two experiments) were quantified, normalized to actin, and are presented as mean ± SEM. **D** and **E,** THBS1 Western blot analysis results of five biological replicates (across two experiments) and THBS2 Western blot analysis results of 5 to 10 biological replicates (across three experiments) were quantified, normalized to actin, and are presented as mean ± SEM. Two-tailed Student *t* test was used for statistical analysis in **C–E**. **F–K,** WT and *Hsf1* null MEFs were co-cultured with N87-GFP cells for 72 hours, and each cell type was grown in mono-culture as control. Co-cultures were sorted by flow cytometry using GFP. **F–H,** The levels of the indicated genes in (GFP-negative) MEFs were determined by qPCR. Average expression in six to eight biological replicates (across three experiments for *INHBA* and *THBS1* and two experiments for *THBS2*), normalized to *HPRT*, ± SEM are presented. Two-way ANOVA was used for statistical analysis. **I,** Representative GFP (top), and brightfield (bottom) images of mono and co-cultures are shown. $N = 3$ biological replicates. Scale bar = 50 μm. **J,** Representative FACS plots showing the percentage of N87-GFP cells co-cultured with WT (left) and *Hsf1* null MEFs (right). $N = 3$ biological replicates. **K,** The average percentage (±SEM) of N87-GFP cells co-cultured with WT and *Hsf1* null MEFs in three biological replicates is shown. Two-tailed Student *t* test was used for statistical analysis. **L–N,** HFF cells treated with siHSF1, siINHBA, siHSF1-INHBA-THBS2 (siCombined), or siControl as indicated were co-cultured with N87-GFP cells for 72 hours. The percentage of N87-GFP in the co-cultures averaged across five to nine biological replicates (±SEM; across three experiments for siINHBA and siHSF1-INHBA-THBS2 and two experiments for siHSF1) is shown. Two-tailed Student *t* test was used for statistical analysis.

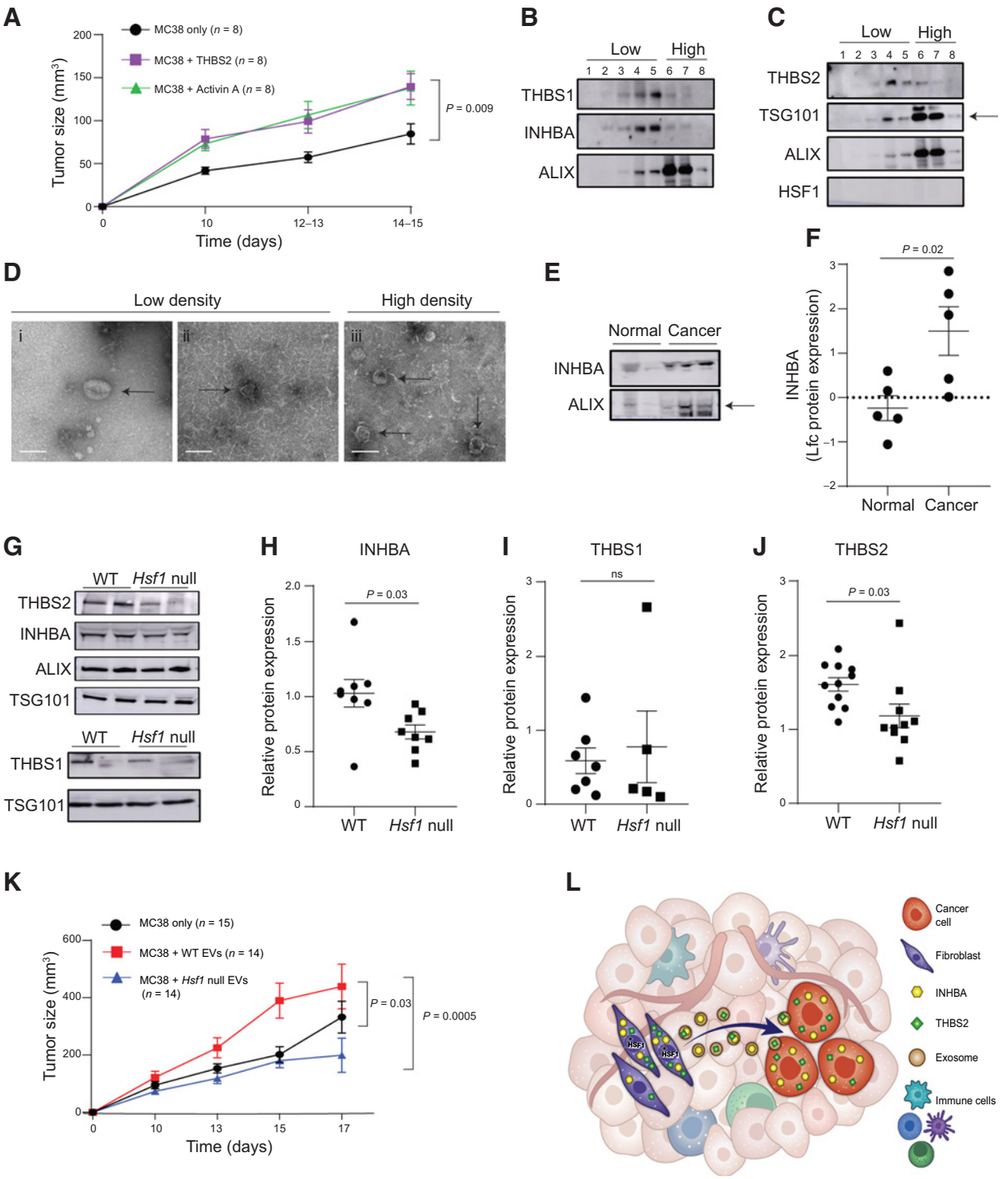

Figure 6.

Fibroblast-derived EVs promote tumor growth in an HSF1-dependent manner. **A,** Nude mice were injected subcutaneously with MC38 cancer cells alone, or co-injected with either recombinant THBS2 or Activin A followed by another injection of recombinant protein 2 days later. Tumor size measured by caliper is presented as mean ± SEM for $N = 8$ mice per group (across two experiments). Repeated measures two-way ANOVA using least-squares means to adjust for group pairwise comparisons was used for statistical analysis. **B** and **C,** Western blot analysis of fractions obtained from Optiprep density gradient isolation of EVs secreted by WT MEFs blotted against exosomal markers ALIX and TSG101, as well as THBS1/2, INHBA, and HSF1. EVs from three WT MEFs were pooled together for the isolation. The experiment was repeated twice (with different biological replicates), representative results are shown. **D,** Representative TEM images of low (i–ii) and high (iii) density EV fractions (repeated two times, from two biological replicates). (*Continued on the following page.*)

tissue exhibited low INHBA, THBS1, and HSF1 staining (**Fig. 4D**). To test whether HSF1 regulates INHBA and THBS1/2 stromal expression, and whether this regulation affects cancer cells, we measured the expression of INHBA and THBS1/2 in WT versus *Hsf1* null mouse embryonic fibroblasts (MEF). THBS1/2 and INHBA protein levels were significantly higher in WT MEFs compared with *Hsf1* null MEFs (**Fig. 5A–E**). Next, we asked if INHBA and THBS1/2 expression in fibroblasts is affected by co-culture with cancer cells. Seventy-two hours of co-culture with N87 human gastric cancer cells led to a significant increase in *Inhba, Thbs1*, and *Thbs2* mRNA levels compared with cells grown in mono-culture (**Fig. 5F–H**). Some induction was also observed in *Hsf1* null MEFs upon co-culture, however the total levels were lower in *Hsf1* null MEFs compared with WT MEFs (**Fig. 5F–H**).

To determine how this stromal network affects cancer cells, we monitored cancer cell growth in co-culture. N87 cells showed a significant growth reduction when co-cultured with *Hsf1* null MEFs compared with WT MEFs (**Fig. 5I–K**), and similar results were observed upon co-culture of N87 cells with human foreskin fibroblasts (HFF) in which HSF1 was knocked down by siRNA (**Fig. 5L**; Supplementary Figs. S5A–S5C).

Next, we knocked down *INHBA, THBS1*, and *THBS2* in fibroblasts and monitored gastric cancer cell growth in co-culture. Knockdown of *THBS2* in HFFs led to a minor decrease in N87 cell proliferation, and knockdown of *THBS1* led to a minor increase in N87 proliferation (Supplementary Figs. S5D–S5F). Knockdown of *INHBA* however led to a substantial and significant decrease in the growth of co-cultured N87 cells (**Fig. 5M**; Supplementary Fig. S5G). A combined knockdown of *HSF1–INHBA–THBS2* had a similar effect on N87 growth (**Fig. 5N**), whereas the combination of *HSF1* and *INHBA* with *THBS1* had a milder effect (Supplementary Fig. S5H). Collectively, these results support the hypothesis that HSF1, INHBA, and THBS1/2 are part of a common stromal protumorigenic signaling network, in which HSF1 regulates the expression of *THBS1/2* and *INHBA*. Although INHBA and THBS2 seem to play a protumorigenic role in fibroblasts, THBS1 may be antitumorigenic.

THBS2 and INHBA are secreted from fibroblasts via EVs, in an HSF1-dependent manner

INHBA and THBS1/2 are secreted proteins (42). We therefore hypothesized that INHBA and THBS2 are secreted from CAFs to the TME where they act on cancer cells, and that this process could be mimicked by exogenous treatment with recombinant proteins. To test this, we co-injected MC38 colon cancer cells with recombinant proteins into mice, subcutaneously, followed by another injection of recombinant protein 2 days later, and monitored tumor growth. Co-injection of either THBS2 or Activin A (a homodimer of two INHBA subunits; ref. 31) with MC38 cancer cells significantly increased the tumorigenicity of these cells—larger and faster growing tumors formed in the presence of THBS2 or Activin A (**Fig. 6A**).

INHBA and THBS1/2 have been proposed to shuttle through EVs (43–49). Recently, THBS2 was shown to be a marker for exosomes secreted by tumors (50). We therefore hypothesized that the protumorigenic effects of stromal HSF1 may be mediated by secretion and delivery of these proteins to the TME, possibly via EVs. Small EVs are lipid bilayer-enclosed particles sized 30 to 150 nm, which mediate cell–cell communication via targeting, fusion, and release of content from one cell to another (51). Their cargo includes bioactive molecules such as effector proteins, metabolites, large and small RNAs, and even genomic DNA (50). Recently, EVs secreted from stromal cells were shown to contribute to disease progression and poor disease outcome by promoting vascularization and chemotherapy resistance (52). To test whether INHBA and THBS1/2 are secreted via EVs in an HSF1-dependent manner, we first confirmed the presence of INHBA and THBS1/2 in EVs by OptiPrep density gradient isolation of EVs secreted from WT MEFs (**Fig. 6B** and **C**; Supplementary Fig. S6A). ALIX and TSG101, two known exosome markers, were used as positive loading controls (53). HSF1 is not expected to be found in EVs and therefore served as a negative control. ALIX and TSG101 were found in fractions 3 to 8. Both proteins peaked in high density fractions (6–7), and TSG101 had an additional peak in low density fraction 4 (**Fig. 6B** and **C**). HSF1 was not detected in any of these fractions. INHBA and THBS1/2, however, were detected in fractions 2 to 7, and peaked in fractions 4 to 5 (**Fig. 6B** and **C**). To confirm that these fractions contain EVs, we performed transmission electron microscope (TEM) analysis. We found that EVs are indeed observed in both low- and high-density fractions (**Fig. 6D**). These observations suggest that two populations of EVs are secreted by MEFs—a low-density population, enriched in INHBA and THBS1/2 (Supplementary Fig. S6A) and a high-density population with lower levels of INHBA and THBS1/2. We also checked the presence of INHBA and THBS1/2 in EVs isolated from the serum of iLgr5;GLI2A mice. Although we could not detect THBS1/2 in the serum (possibly due to low sensitivity of the assay), INHBA was detected, and its levels were significantly higher in EVs isolated from the serum of tumor-bearing iLgr5;GLI2A mice compared with EVs isolated from the serum of naïve iLgr5;GLI2A mice (**Fig. 6E** and **F**).

We then compared the expression levels of INHBA and THBS1/2 in EVs isolated from WT versus *Hsf1* null fibroblasts. Although THBS1 levels were similar between WT and *Hsf1* null-derived EVs, THBS2 and INHBA levels were significantly higher in EVs derived from WT MEFs compared with EVs from *Hsf1* null MEFs (**Fig. 6G–J**). These results suggest that INHBA and THBS2 expression in EVs is HSF1-dependent.

To examine whether the differential expression of INHBA and THBS2 was due to impaired EV biogenesis in *Hsf1* null MEFs, we compared the number and size of EVs produced by each genotype

(*Continued.*) (i) 1.03% sucrose; (ii) 1.04% sucrose; (iii) 1.07% sucrose. Scale bars = 100 nm. **E,** Representative Western blot analysis showing INHBA levels from EVs isolated from the serum of tumor-bearing and naïve iLgr5;GLI2A mice. ALIX was used as loading control. Arrow indicates expected size of ALIX. **F,** INHBA levels from EVs isolated from the serum of tumor-bearing and naïve iLgr5;GLI2A mice were analyzed using Western blot analysis. INHBA levels were normalized to ALIX. Average expression of INHBA normalized to ALIX in five biological replicates (across two experiments) is presented in as mean ± SEM. Two-tailed Student *t* test was used for statistical analysis. **G–J,** INHBA, THBS1, and THBS2 levels in EVs derived from WT and *Hsf1* null primary MEFs were analyzed using Western blot analysis. ALIX and TSG101 were used as loading controls. Representative blots are shown in **G**. **H,** Average expression of INHBA normalized to TSG101 in eight biological replicates (across three experiments for INHBA) is presented as mean ± SEM. **I,** Average expression of THBS1 normalized to TSG101 in five to seven biological replicates (across three experiments) is presented as mean ± SEM. **J,** Average expression THBS2 normalized to TSG101 in 10 to 11 biological replicates (across four experiments) is presented as mean ± SEM. Two-tailed Student *t* test was used for statistical analysis in **H** and **I**. **K,** Nude mice were injected subcutaneously with MC38 cancer cells alone, or co-injected with EVs derived from WT or *Hsf1* null MEFs. Tumor size measured by caliper is presented as mean ± SEM for $N = 14$ to 15 mice per group (across four experiments). Repeated measures two-way ANOVA using least-squares means to adjust for group pairwise comparisons was used for statistical analysis. **L,** Graphic summary of the proposed model. HSF1 in CAFs regulates expression of INHBA and THBS1/2. INHBA and THBS2 from CAFs are packaged into EVs and secreted to the TME, where they are taken up by cancer cells.

using nanoparticle tracking analysis (NTA). We could not detect differences in size or in quantity between EVs secreted from WT and *Hsf1* null fibroblasts (Supplementary Figs. S6B–S6E). We extended our analysis to field-flow fractionation (FFF), to better separate EV populations and assess smaller EV populations shown to be biologically active (54). Similar to our NTA analysis, FFF did not detect consistent differences between EVs derived from *Hsf1* null MEFs compared with WT MEFs (Supplementary Fig. S6F). We next tested whether the differences in protein content could be due to impaired uptake of EVs derived from *Hsf1* null compared with WT MEFs. We incubated N87 gastric cancer cells and MC38 colon cancer cells with CFSE stained EVs, and analyzed uptake 12 to 16 hours later by imaging the cells in an ImageStream imaging flow cytometer. We could not detect differences in the percentage of $CFSE^+$ N87 and MC38 cells incubated in the presence of EVs from *Hsf1* null compared with WT MEFs (Supplementary Figs. S6G–S6O), indicating that HSF1 does not affect EV biogenesis or uptake, yet it plays an important role in the protein content of EVs.

To assess the biological relevance of these findings we co-injected EVs derived from WT versus *Hsf1* null MEFs together with MC38 cancer cells into nude mice, and monitored tumor growth. Co-injection with EVs derived from WT MEFs caused a significant increase in the growth of MC38-injected tumors (**Fig. 6K**). This effect was completely abolished when EVs from *Hsf1* null MEFs were co-injected with MC38 cells. Taken together these experiments show that EVs derived from WT and *Hsf1* null MEFs are similar in size, quantity, biogenesis, and uptake into cancer cells. However, there is a significant difference in their content and, consequently, their effect on tumor growth. These findings imply that HSF1 regulates the expression of INHBA and THBS1/2 in stromal cells. INHBA and THBS2 are then packaged into EVs in an HSF1-dependent manner and secreted to the TME, where they are taken up by cancer cells and promote a more aggressive disease phenotype (**Fig. 6L**).

Discussion

Despite recent advances in molecular subtyping, the backbone of gastric cancer treatment remains chemotherapeutic combinations. Molecular classifications, based largely on mutations and genomic alterations in the cancer cells, do not translate to guide treatment modality. Here we chose a complementary approach—searching for transcriptional changes in the gastric TME. We defined a stromal gene signature associated with poor disease outcome in patients, and found a role for the stromal master transcriptional regulator HSF1 in driving it, through exosome-mediated secretion of protumorigenic proteins that are taken up by cancer cells to promote aggressive disease phenotypes.

HSF1 was previously shown by us and others to play protumorigenic roles in CAFs of breast, lung, and colon carcinomas (17, 20, 38). The finding that HSF1 also acts in gastric CAFs implicates HSF1 as a master regulator of CAF activities in carcinomas across different tissues, and suggests that its protumorigenic effects—in gastric cancer and other carcinomas—may be mediated via delivery of targets to the TME in EVs.

INHBA and THBS1/2 are involved in tumor progression and were shown to be co-regulated (30, 55, 56) possibly sharing common signaling pathways. Although INHBA and THBS2 are protumorigenic, THBS1 was proposed to exert both pro- and antitumorigenic effects, depending on the system examined (44, 55, 57). Our findings suggest that all three proteins are upregulated in CAFs in an HSF1-dependent manner. Our *in vitro* experiments and mouse co-injections with recombinant proteins show a clear protumorigenic role of Activin A and THBS2, whereas the effect of stromal THBS1 on cancer cells (*in vitro*) is less clear. Taken together with the finding that INHBA and THBS2 are delivered into exosomes in an HSF1-dependent manner, whereas THBS1 exosomal expression is not affected by HSF1 status, it is possible that selective delivery of INHBA and THBS2 to exosomes leads to the protumorigenic effect observed, whereas THBS1 is antitumorigenic.

EV cargo includes proteins, metabolites, RNA, and genomic DNA (50), which could serve as bioactive molecules in the TME. In GI-tract cancers, EVs from CAFs were shown to promote cancer through delivery of miRNAs to gastric cancer cells to suppress ferroptosis (58), and Wnt glycoproteins to colorectal cancer cells to induce cancer stemness and chemoresistance (59). In our study, differential protein expression in EVs affects their activity. Although biogenesis and uptake of EVs was not impaired, loss of HSF1 abolished the protumorigenic effect of EVs derived from WT MEFs. Our findings indicate that EV cargo is selective and the content is affected by HSF1.

Over the last years, efforts were made to identify gastric cancer drivers and gene signatures that may serve as biomarkers for diagnosis and treatment (3). Trastuzumab revolutionized the treatment of HER2-positive gastric cancers (60), and immunotherapy has proven to be an effective therapy for patients with microsatellite instability (MSI; ref. 61). Other signatures, such as those associated with *Helicobacter pylori* and *EBV* infections (62, 63), germline mutations of *CDH1*, mismatch repair genes (64, 65), epithelial versus mesenchymal cell types (5), and MSS $TP53^-$, MSS $TP53^+$, MSI, EMT subtypes (4) enabled associations between molecular landscape and gastric cancer subtyping (3, 60). However, the TME of gastric cancer in general, and the molecular composition of gastric CAFs in particular, have been scarcely studied. Our profiling of CAFs from patient tumors highlights stromal compositions associated with the aggressive diffuse and EMT-like gastric cancer subtypes. These targets should be further explored, certainly as prognostic targets and hopefully as robust therapeutic targets in gastric cancer.

Authors' Disclosures

No disclosures were reported.

Authors' Contributions

N. Grunberg: Formal analysis, investigation, writing–original draft, writing–review and editing. **M. Pevsner-Fischer:** Formal analysis, investigation, writing–original draft, writing–review and editing. **T. Goshen-Lago:** Resources. **J. Diment:** Formal analysis, visualization. **Y. Stein:** Formal analysis, methodology. **H. Lavon:** Investigation. **S. Mayer:** Data curation, formal analysis, methodology. **O. Levi-Galibov:** Resources, formal analysis, investigation. **G. Friedman:** Resources, investigation, methodology. **Y. Ofir-Birin:** Data curation, visualization, methodology. **L. Syu:** Resources. **C. Migliore:** Resources. **E. Shimoni:** Resources, visualization, methodology. **S.M. Stemmer:** Resources, data curation, methodology, writing–review and editing. **B. Brenner:** Resources, methodology, writing-review and editing. **A.A. Dlugosz:** Resources, writing–review and editing. **D. Lyden:** Conceptualization, data curation, supervision, investigation, methodology, writing–original draft, writing–review and editing. **N. Regev-Rudzki:** Formal analysis, methodology, writing–review and editing. **I. Ben-Aharon:** Resources, formal analysis, investigation, writing–review and editing. **R. Scherz-Shouval:** Conceptualization, supervision, investigation, methodology, writing–original draft, writing–review and editing.

Acknowledgments

Mouse pathological evaluation was carried out by Ori Brenner (WIS). Bioinformatic analyses were assisted by Ester Feldmesser, Ron Rotkopf, and Irit Orr (WIS). We thank Raya Eilam-Altstadter for assistance with immunostaining, Andreas Moor for guidance with LCM, Rawand Hamodi for technical assistance, and members of the

Scherz-Shouval lab for their valuable input. R. Scherz-Shouval was supported by ISF grants 401/17 and 1384/1, ERC grant 754320, the Israel cancer research fund, the Abisch-Frenkel foundation, the Laura Gurwin Flug Family Fund, the Peter and Patricia Gruber Awards, the Comisaroff Family Trust, the Estate of Annice Anzelewitz, and the Estate of Mordecai M. Roshwal. R. Scherz-Shouval was the incumbent of the Ernst and Kaethe Ascher Career Development Chair in Life Sciences. A.A. Dlugosz was supported by NIH grants R01 CA118875 and P30 CA046592.

The costs of publication of this article were defrayed in part by the payment of page charges. This article must therefore be hereby marked *advertisement* in accordance with 18 U.S.C. Section 1734 solely to indicate this fact.

Received August 19, 2020; revised December 22, 2020; accepted February 1, 2021; published first xx xx, xxxx.

References

1. Corso S, Isella C, Bellomo SE, Apicella M, Durando S, Migliore C, et al. A comprehensive PDX gastric cancer collection captures cancer cell-intrinsic transcriptional MSI traits. Cancer Res 2019;79:5884–96.
2. Lordick F, Allum W, Carneiro F, Mitry E, Tabernero J, Tan P, et al. Unmet needs and challenges in gastric cancer: the way forward. Cancer Treat Rev 2014;40:692–700.
3. Cancer Genome Atlas Research N. Comprehensive molecular characterization of gastric adenocarcinoma. Nature 2014;513:202–9.
4. Cristescu R, Lee J, Nebozhyn M, Kim KM, Ting JC, Wong SS, et al. Molecular analysis of gastric cancer identifies subtypes associated with distinct clinical outcomes. Nat Med 2015;21:449–56.
5. Oh SC, Sohn BH, Cheong JH, Kim SB, Lee JE, Park KC, et al. Clinical and genomic landscape of gastric cancer with a mesenchymal phenotype. Nat Commun 2018;9:1777.
6. Tan IB, Ivanova T, Lim KH, Ong CW, Deng NT, Lee J, et al. Intrinsic subtypes of gastric cancer, based on gene expression pattern, predict survival and respond differently to chemotherapy. Gastroenterology 2011;141:476–U551.
7. Van Cutsem E, Sagaert X, Topal B, Haustermans K, Prenen H. Gastric cancer. Lancet 2016;388:2654–64.
8. Becker KF, Keller G, Hoefler H. The use of molecular biology in diagnosis and prognosis of gastric cancer. Surg Oncol 2000;9:5–11.
9. Tabassum DP, Polyak K. Tumorigenesis: it takes a village. Nat Rev Cancer 2015; 15:473–83.
10. Hanahan D, Coussens LM. Accessories to the crime: functions of cells recruited to the tumor microenvironment. Cancer Cell 2012;21:309–22.
11. Morihiro T, Kuroda S, Kanaya N, Kakiuchi Y, Kubota T, Aoyama K, et al. PD-L1 expression combined with microsatellite instability/CD8+ tumor infiltrating lymphocytes as a useful prognostic biomarker in gastric cancer. Sci Rep 2019;9:4633.
12. Sahai E, Astsaturov I, Cukierman E, DeNardo DG, Egeblad M, Evans RM, et al. A framework for advancing our understanding of cancer-associated fibroblasts. Nat Rev Cancer 2020;20:174–86.
13. Erez N, Truitt M, Olson P, Arron ST, Hanahan D. Cancer-associated fibroblasts are activated in incipient neoplasia to orchestrate tumor-promoting inflammation in an NF-kappa B-dependent manner (vol 17, pg 135, 2010). Cancer Cell 2010;17:523.
14. Finak G, Bertos N, Pepin F, Sadekova S, Souleimanova M, Zhao H, et al. Stromal gene expression predicts clinical outcome in breast cancer. Nat Med 2008;14: 518–27.
15. Kalluri R. The biology and function of fibroblasts in cancer. Nat Rev Cancer 2016; 16:582–98.
16. Friedman G, Levi-Galibov O, David E, Bornstein C, Giladi A, Dadiani M, et al. Cancer-associated fibroblast compositions change with breast-cancer progression linking S100A4 and PDPN ratios with clinical outcome. Nature Cancer 2020.
17. Levi-Galibov O, Lavon H., Wassermann-Dozorets R., et al. Heat Shock Factor 1-dependent extracellular matrix remodeling mediates the transition from chronic intestinal inflammation to colon cancer. Nat Commun 2020;11:6245.
18. Zhi KK, Shen XJ, Zhang H, Bi JW. Cancer-associated fibroblasts are positively correlated with metastatic potential of human gastric cancers. J Exp Clin Canc Res 2010;29:66.
19. Li BL, Jiang YM, Li GX, Fisher GA, Li RJ. Natural killer cell and stroma abundance are independently prognostic and predict gastric cancer chemotherapy benefit. JCI Insight 2020;5:e136570.
20. Scherz-Shouval R, Santagata S, Mendillo ML, Sholl LM, Ben-Aharon I, Beck AH, et al. The reprogramming of tumor stroma by HSF1 is a potent enabler of malignancy. Cell 2014;158:564–78.
21. Syu LJ, Zhao X, Zhang Y, Grachtchouk M, Demitrack E, Ermilov A, et al. Invasive mouse gastric adenocarcinomas arising from Lgr5+ stem cells are dependent on crosstalk between the Hedgehog/GLI2 and mTOR pathways. Oncotarget 2016;7: 10255–70.
22. McMillan DR, Xiao XZ, Shao L, Graves K, Benjamin IJ. Targeted disruption of heat shock transcription factor 1 abolishes thermotolerance and protection against heat-inducible apoptosis. J Biol Chem 1998;273:7523–8.
23. Yohai VJ, Zamar RH. High breakdown-point estimates of regression by means of the minimization of an efficient scale. J Am Stat Assoc 1988;83:406–13.
24. Maronna RA, Zamar RH. Robust estimates of location and dispersion for high-dimensional datasets. Technometrics 2002;44:307–17.
25. Gnanadesikan R, Kettenring JR. Robust estimates, residuals, and outlier detection with multiresponse data. Biometrics 1972;28:81.
26. Love MI, Huber W, Anders S. Moderated estimation of fold change and dispersion for RNA-seq data with DESeq2. Genome Biol 2014;15:550.
27. Jaitin DA, Kenigsberg E, Keren-Shaul H, Elefant N, Paul F, Zaretsky I, et al. Massively parallel single-cell RNA-seq for marker-free decomposition of tissues into cell types. Science 2014;343:776–9.
28. Maruyama S, Furuya S, Shiraishi K, Shimizu H, Akaike H, Hosomura N, et al. Podoplanin expression as a prognostic factor in gastric cancer. Anticancer Res 2018;38:2717–22.
29. Shindo K, Aishima S, Ohuchida K, Fujiwara K, Fujino M, Mizuuchi Y, et al. Podoplanin expression in cancer-associated fibroblasts enhances tumor progression of invasive ductal carcinoma of the pancreas. Mol Cancer 2013;12:168.
30. Kim H, Watkinson J, Varadan V, Anastassiou D. Multi-cancer computational analysis reveals invasion-associated variant of desmoplastic reaction involving INHBA, THBS2 and COL11A1. BMC Med Genomics 2010;3:51.
31. Link AS, Zheng F, Alzheimer C. Activin signaling in the pathogenesis and therapy of neuropsychiatric diseases. Front Mol Neurosci 2016;7.
32. Namwanje M, Brown CW. Activins and inhibins: roles in development, physiology, and disease. Cold Spring Harb Perspect Biol 2016;8:a021881.
33. Seeruttun SR, Cheung WY, Wang W, Fang C, Liu ZM, Li JQ, et al. Identification of molecular biomarkers for the diagnosis of gastric cancer and lymph-node metastasis. Gastroenterol Rep (Oxf) 2019;7:57–66.
34. Oue N, Aung PP, Mitani Y, Kuniyasu H, Nakayama H, Yasui W. Genes involved in invasion and metastasis of gastric cancer identified by array-based hybridization and serial analysis of gene expression. Oncology 2005;69:17–22.
35. Hong BB, Chen SQ, Qi YL, Zhu JW, Lin JY. Association of THBS1 rs1478605 T>C in 5'-untranslated regions with the development and progression of gastric cancer. Biomed Rep 2015;3:207–14.
36. Huang T, Wang L, Liu D, Li P, Xiong H, Zhuang L, et al. FGF7/FGFR2 signal promotes invasion and migration in human gastric cancer through upregulation of thrombospondin-1. Int J Oncol 2017;50:1501–12.
37. Sun C, Yuan Q, Wu D, Meng X, Wang B. Identification of core genes and outcome in gastric cancer using bioinformatics analysis. Oncotarget 2017;8: 70271–80.
38. Ferrari N, Ranftl R, Chicherova I, Slaven ND, Moeendarbary E, Farrugia AJ, et al. Dickkopf-3 links HSF1 and YAP/TAZ signalling to control aggressive behaviours in cancer-associated fibroblasts. Nat Commun 2019;10:130.
39. Mendillo ML, Santagata S, Koeva M, Bell GW, Hu R, Tamimi RM, et al. HSF1 drives a transcriptional program distinct from heat shock to support highly malignant human cancers. Cell 2012;150:549–62.
40. Kovacs D, Sigmond T, Hotzi B, Bohar B, Fazekas D, Deak V, et al. HSF1Base: a comprehensive database of HSF1 (heat shock factor 1) target genes. Int J Mol Sci 2019;20:5815.
41. Dai W, Ye J, Zhang Z, Yang L, Ren H, Wu H, et al. Increased expression of heat shock factor 1 (HSF1) is associated with poor survival in gastric cancer patients. Diagn Pathol 2018;13:80.
42. Uhlen M, Fagerberg L, Hallstrom BM, Lindskog C, Oksvold P, Mardinoglu A, et al. Proteomics. Tissue-based map of the human proteome. Science 2015;347: 1260419.

43. Becker A, Thakur BK, Weiss JM, Kim HS, Peinado H, Lyden D. Extracellular vesicles in cancer: cell-to-cell mediators of metastasis. Cancer Cell 2016;30: 836–48.
44. Huang WT, Chong IW, Chen HL, Li CY, Hsieh CC, Kuo HF, et al. Pigment epithelium-derived factor inhibits lung cancer migration and invasion by upregulating exosomal thrombospondin 1. Cancer Lett 2019;442:287–98.
45. Morhayim J, van de Peppel J, Demmers JA, Kocer G, Nigg AL, van Driel M, et al. Proteomic signatures of extracellular vesicles secreted by nonmineralizing and mineralizing human osteoblasts and stimulation of tumor cell growth. FASEB J 2015;29:274–85.
46. Sobral LM, Bufalino A, Lopes MA, Graner E, Salo T, Coletta RD. Myofibroblasts in the stroma of oral cancer promote tumorigenesis via secretion of activin A. Oral Oncol 2011;47:840–6.
47. Stenina OI, Topol EJ, Plow EF. Thrombospondins, their polymorphisms, and cardiovascular disease. Arterioscler Thromb Vasc Biol 2007; 27:1886–94.
48. Xiao M, Zhang J, Chen W, Chen W. M1-like tumor-associated macrophages activated by exosome-transferred THBS1 promote malignant migration in oral squamous cell carcinoma. J Exp Clin Cancer Res 2018;37:143.
49. Zhang XW, Zhou JC, Peng D, Hua F, Li K, Yu JJ, et al. Disrupting the TRIB3-SQSTM1 interaction reduces liver fibrosis by restoring autophagy and suppressing exosome-mediated HSC activation. Autophagy 2020;16:782–96.
50. Hoshino A, Kim HS, Bojmar L, Gyan KE, Cioffi M, Hernandez J, et al. Extracellular vesicle and particle biomarkers define multiple human cancers. Cell 2020;182:1044–61.
51. van Niel G, D'Angelo G, Raposo G. Shedding light on the cell biology of extracellular vesicles. Nat Rev Mol Cell Biol 2018;19:213–28.
52. Boelens MC, Wu TJ, Nabet BY, Xu B, Qiu Y, Yoon T, et al. Exosome transfer from stromal to breast cancer cells regulates therapy resistance pathways. Cell 2014; 159:499–513.
53. Willms E, Johansson HJ, Mager I, Lee Y, Blomberg KE, Sadik M, et al. Cells release subpopulations of exosomes with distinct molecular and biological properties. Sci Rep 2016;6:22519.
54. Zhang H, Freitas D, Kim HS, Fabijanic K, Li Z, Chen H, et al. Identification of distinct nanoparticles and subsets of extracellular vesicles by asymmetric flow field-flow fractionation. Nat Cell Biol 2018;20:332–43.
55. Wang X, Zhang L, Li H, Sun WJ, Zhang HH, Lai MD. THBS2 is a potential prognostic biomarker in colorectal cancer. Sci Rep-Uk 2016;6:33366.
56. Weng TY, Wang CY, Hung YH, Chen WC, Chen YL, Lai MD. Differential expression pattern of THBS1 and THBS2 in lung cancer: clinical outcome and a systematic-analysis of microarray databases. PLoS One 2016;11:e0161007.
57. Kashihara H, Shimada M, Yoshikawa K, Higashijima J, Tokunaga T, Nishi M, et al. Correlation between thrombospondin-1 expression in non-cancer tissue and gastric carcinogenesis. Anticancer Res 2017;37:3547–52.
58. Zhang H, Deng T, Liu R, Ning T, Yang H, Liu D, et al. CAF secreted miR-522 suppresses ferroptosis and promotes acquired chemo-resistance in gastric cancer. Mol Cancer 2020;19:43.
59. Hu YB, Yan C, Mu L, Mi YL, Zhao H, Hu H, et al. Exosomal Wnt-induced dedifferentiation of colorectal cancer cells contributes to chemotherapy resistance. Oncogene 2019;38:1951–65.
60. Gunturu KS, Woo Y, Beaubier N, Remotti HE, Saif MW. Gastric cancer and trastuzumab: first biologic therapy in gastric cancer. Ther Adv Med Oncol 2013; 5:143–51.
61. Yuza K, Nagahashi M, Watanabe S, Takabe K, Wakai T. Hypermutation and microsatellite instability in gastrointestinal cancers. Oncotarget 2017;8: 112103–15.
62. Uemura N, Okamoto S, Yamamoto S, Matsumura N, Yamaguchi S, Yamakido M, et al. Helicobacter pylori infection and the development of gastric cancer. N Engl J Med 2001;345:784–9.
63. Zhao Y, Zhang J, Cheng ASL, Yu J, To KF, Kang W. Gastric cancer: genome damaged by bugs. Oncogene 2020;39:3427–42.
64. Keller G, Grimm V, Vogelsang H, Bischoff P, Mueller J, Siewert JR, et al. Analysis for microsatellite instability and mutations of the DNA mismatch repair gene hMLH1 in familial gastric cancer. Int J Cancer 1996;68:571–6.
65. Richards FM, McKee SA, Rajpar MH, Cole TR, Evans DG, Jankowski JA, et al. Germline E-cadherin gene (CDH1) mutations predispose to familial gastric cancer and colorectal cancer. Hum Mol Genet 1999;8:607–10.